This supplemental information file covers: (1) Contribution analysis results for the laboratory-scale perovskite tandems; (2) Contribution analysis results for the commercial-scale perovskite tandems; (3) Resistivity test results; (4) Short current density, open circuit voltage, and fill factor of perovskite-perovskite tandem; (5) Transmittance; (6) Scanning Electron Microscopy; (7) Normalized photoluminescence (PL) intensity and PL quantum efficiency (PLQE); (8) Solar cell stability test; (9) Cumulative energy yield; (10) Doctor blading v.s. solvent dissolution method; (11) Techno-economic analysis for the recovery process with sensitivity analysis; (12) Impact of module shipping; (13) Sensitivity analysis of EROI on insolation condition; (14) Impact of PCE threshold on perovskite-perovskite tandem module replacement; (15) Material and energy inventory; (16) Supplemental references.

Supplemental items

Contribution analysis results for the laboratory-scale perovskite tandems

Two representative perovskite tandem architectures that have the potential to be implemented on a commercial scale are investigated. Identifying the energy and environmental hotspots from the prototypical tandem architectures through contribution analysis is important and guides material and processing step replacement toward industry-relevant tandem stacks. The results of the “cradle-to-grave” contribution analysis would inform the components worth recycling and guide the experimental investigation of the recycling process at the laboratory scale. The “cradle-to-grave” system boundary comprises four life cycle stages, including raw material acquisition, device fabrication, electricity generation, and end-of-life disposal. The landfill of used photovoltaic (PV) modules is selected as the end-of-life scenario method following the existing literature. The Product Environmental Footprint (PEF) approach is selected to unmask the full spectrum environmental profiles of the investigated perovskite tandem modules.[1] There is a total of 17 midpoint indicators, including climate change; ozone depletion; human toxicity, cancer effects; human toxicity, non-cancer effects; particulate matter/respiratory effects; ionizing radiation, human health; photochemical ozone formation; acidification; eutrophication, terrestrial; eutrophication, freshwater; eutrophication, marine; ecotoxicity, freshwater; land use; resource depletion, water; resource depletion, mineral, fossil, renewable; cumulative energy demand (CED), renewable; and CED, non-renewable.

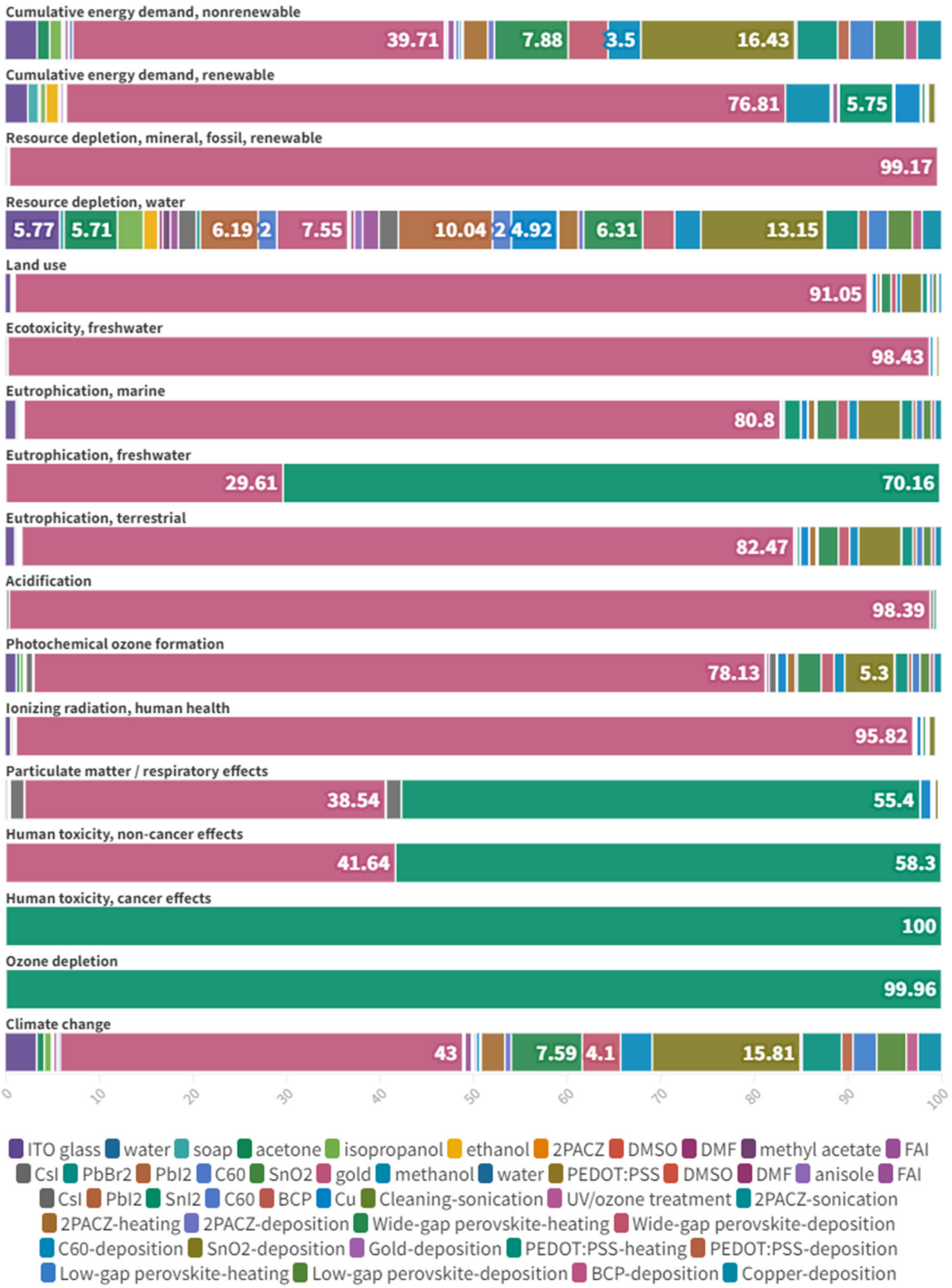
Cumulative energy demand, nonrenewable
39.71
7.88
3.5
16.43
Cumulative energy demand, renewable
76.81
5.75
Resource depletion, mineral, fossil, renewable
99.17
Resource depletion, water
5.77
5.71
6.19
2
7.55
10.04
2
4.92
6.31
13.15
Land use
91.05
Ecotoxicity, freshwater
98.43
Eutrophication, marine
80.8
Eutrophication, freshwater
29.61
70.16
Eutrophication, terrestrial
82.47
Acidification
98.39
Photochemical ozone formation
78.13
5.3
Ionizing radiation, human health
95.82
Particulate matter / respiratory effects
38.54
55.4
Human toxicity, non-cancer effects
41.64
58.3
Human toxicity, cancer effects
100
Ozone depletion
99.96
Climate change
43
7.59
4.1
15.81
0
10
20
30
40
50
60
70
80
90
100
ITO glass
water
soap
acetone
isopropanol
ethanol
2PACZ
DMSO
DMF
methyl acetate
FAI
CsI
PbBr2
PbI2
C60
SnO2
gold
methanol
water
PEDOT:PSS
DMSO
DMF
anisole
FAI
CsI
PbI2
SnI2
C60
BCP
Cu
Cleaning-sonication
UV/ozone treatment
2PACZ-sonication
2PACZ-heating
2PACZ-deposition
Wide-gap perovskite-heating
Wide-gap perovskite-deposition
C60-deposition
SnO2-deposition
Gold-deposition
PEDOT:PSS-heating
PEDOT:PSS-deposition
Low-gap perovskite-heating
Low-gap perovskite-deposition
BCP-deposition
Copper-deposition

29

Figure S1. Contribution analysis results for the laboratory-scale perovskite-perovskite tandem with a "cradle-to-grave" system boundary.

Figure S1 depicts the environmental profile of the laboratory-scale perovskite-perovskite tandem for the explored midpoint impact categories according to the PEF method. The environmental impacts are divided by different material and energy inputs for each impact category. We note that gold and atomic layer deposition (ALD) of the SnO_2 layer are identified as the predominant contributors to cumulative energy demand and climate change. The ALD of the SnO_2 layer is regarded as the primary contributor due to intensive energy consumption, accounting for 31.8% of the total energy consumption.

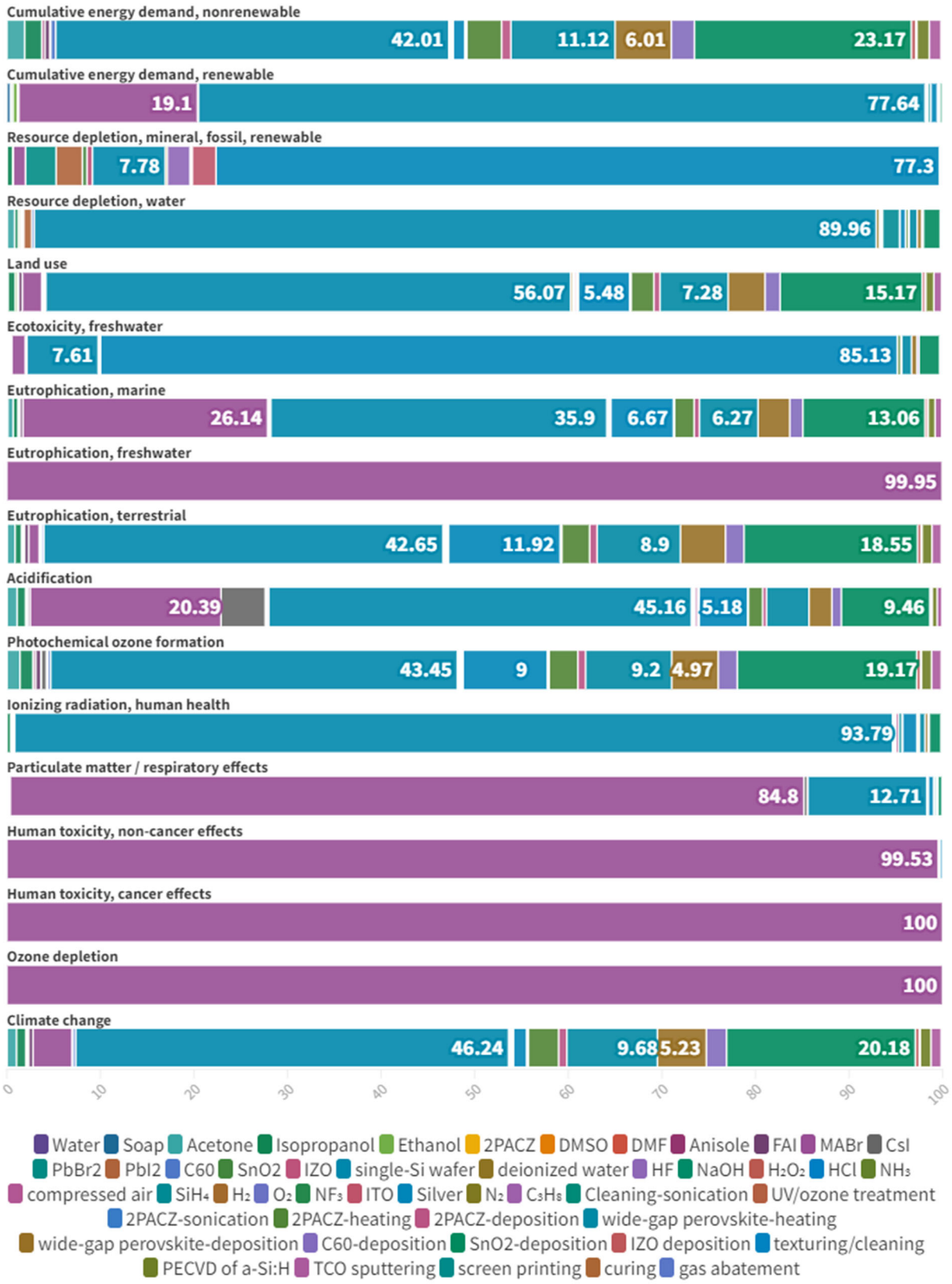
Cumulative energy demand, nonrenewable
42.01
11.12
6.01
23.17
Cumulative energy demand, renewable
19.1
77.64
Resource depletion, mineral, fossil, renewable
7.78
77.3
Resource depletion, water
89.96
Land use
56.07
5.48
7.28
15.17
Ecotoxicity, freshwater
7.61
85.13
Eutrophication, marine
26.14
35.9
6.67
6.27
13.06
Eutrophication, freshwater
99.95
Eutrophication, terrestrial
42.65
11.92
8.9
18.55
Acidification
20.39
45.16
5.18
9.46
Photochemical ozone formation
43.45
9
9.2
4.97
19.17
Ionizing radiation, human health
93.79
Particulate matter / respiratory effects
84.8
12.71
Human toxicity, non-cancer effects
99.53
Human toxicity, cancer effects
100
Ozone depletion
100
Climate change
46.24
9.68
5.23
20.18
0
10
20
30
40
50
60
70
80
90
100
Water
Soap
Acetone
Isopropanol
Ethanol
2PACZ
DMSO
DMF
Anisole
FAI
MABr
CsI
PbBr2
PbI2
C60
SnO2
IZO
single-Si wafer
deionized water
HF
NaOH
H2O2
HCl
NH3
compressed air
SiH4
H2
O2
NF3
ITO
Silver
N2
C3H8
Cleaning-sonication
UV/ozone treatment
2PACZ-sonication
2PACZ-heating
2PACZ-deposition
wide-gap perovskite-heating
wide-gap perovskite-deposition
C60-deposition
SnO2-deposition
IZO deposition
texturing/cleaning
PECVD of a-Si:H
TCO sputtering
screen printing
curing
gas abatement

40

Figure S2. Contribution analysis results for the laboratory-scale perovskite-silicon tandem with a “cradle-to-grave” system boundary.

Figure S2 depicts the full-spectrum environmental profile for the laboratory-scale perovskite-silicon tandem. We note that for most of the impact categories, heating processes, silicon wafers, and ALD of SnO_2 are the significant contributors. In addition, the use of silver contributes up to 80% of the indicator regarding resource depletion and freshwater ecotoxicity. The use of even small quantities of the precious metal dominates certain impact categories for perovskite tandems. The impact of MABr is the most pronounced for human toxicity and ozone depletion.

Contribution analysis results for the commercial-scale perovskite tandems

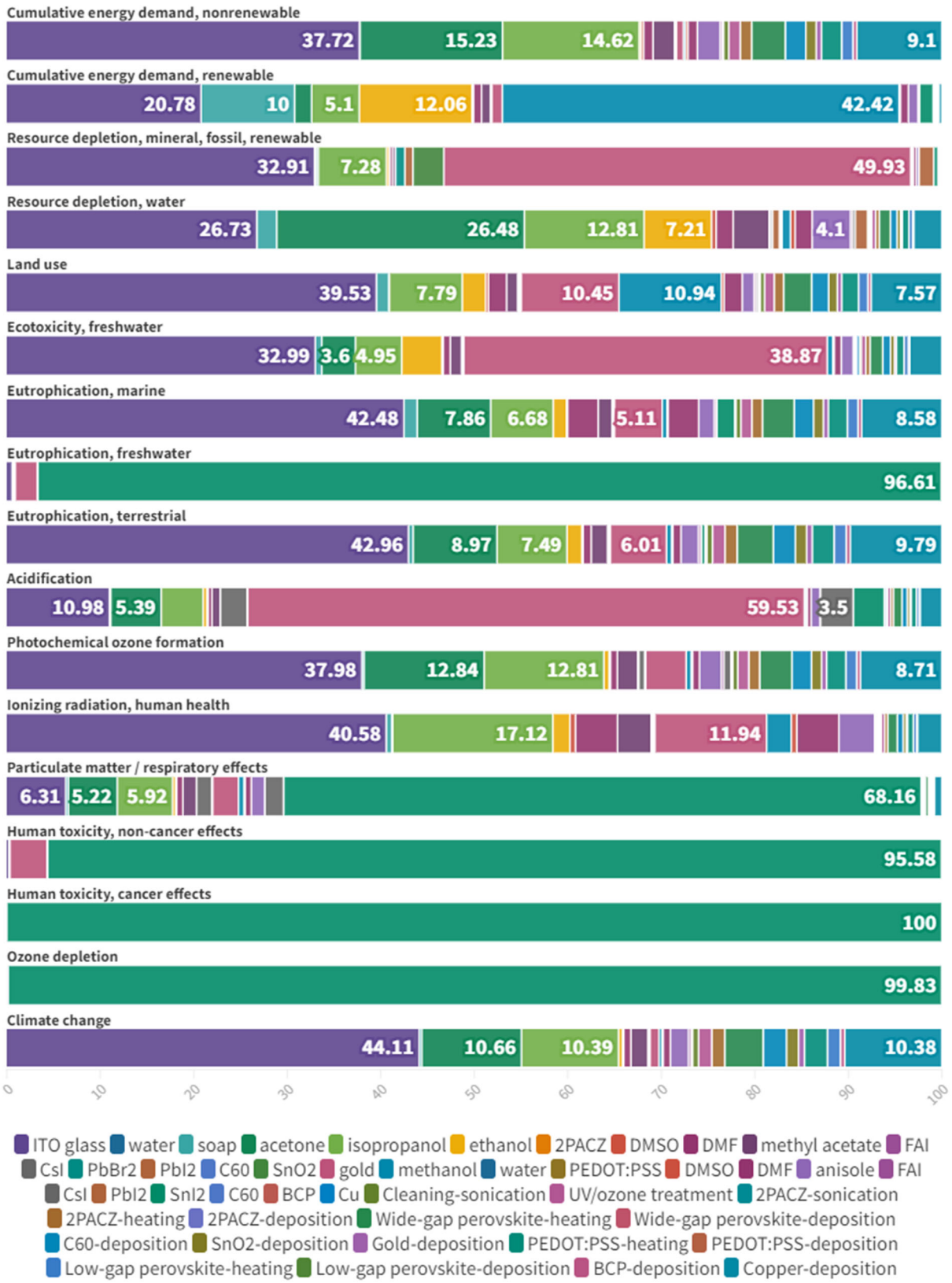
Cumulative energy demand, nonrenewable
37.72
15.23
14.62
9.1
Cumulative energy demand, renewable
20.78
10
5.1
12.06
42.42
Resource depletion, mineral, fossil, renewable
32.91
7.28
49.93
Resource depletion, water
26.73
26.48
12.81
7.21
4.1
Land use
39.53
7.79
10.45
10.94
7.57
Ecotoxicity, freshwater
32.99
3.6
4.95
38.87
Eutrophication, marine
42.48
7.86
6.68
5.11
8.58
Eutrophication, freshwater
96.61
Eutrophication, terrestrial
42.96
8.97
7.49
6.01
9.79
Acidification
10.98
5.39
59.53
3.5
Photochemical ozone formation
37.98
12.84
12.81
8.71
Ionizing radiation, human health
40.58
17.12
11.94
Particulate matter / respiratory effects
6.31
5.22
5.92
68.16
Human toxicity, non-cancer effects
95.58
Human toxicity, cancer effects
100
Ozone depletion
99.83
Climate change
44.11
10.66
10.39
10.38
0
10
20
30
40
50
60
70
80
90
100
ITO glass
water
soap
acetone
isopropanol
ethanol
2PACZ
DMSO
DMF
methyl acetate
FAI
CsI
PbBr2
PbI2
C60
SnO2
gold
methanol
water
PEDOT:PSS
DMSO
DMF
anisole
FAI
CsI
PbI2
SnI2
C60
BCP
Cu
Cleaning-sonication
UV/ozone treatment
2PACZ-sonication
2PACZ-heating
2PACZ-deposition
Wide-gap perovskite-heating
Wide-gap perovskite-deposition
C60-deposition
SnO2-deposition
Gold-deposition
PEDOT:PSS-heating
PEDOT:PSS-deposition
Low-gap perovskite-heating
Low-gap perovskite-deposition
BCP-deposition
Copper-deposition

Figure S3. Contribution analysis results for the commercial-scale perovskite-perovskite tandem with a "cradle-to-grave" system boundary.

To explicitly consider scalable fabrication of the investigated perovskite tandems, we use two tandem architectures in existing literature[2, 3] as references while substituting the materials and processing steps used for depositing specific layers with scalable alternatives.[4] Specifically, spin coating is replaced with screen printing, which is compatible with large-scale and high-throughput manufacturing.[5] The energy-intensive ALD of tin dioxide is replaced with sputtering. Although the industry-relevant ALD process, such as spatial atmospheric ALD,[6] is two times faster than the laboratory-scale counterpart and thus consumes less energy, it is still energy-intensive in terms of absolute energy consumption.

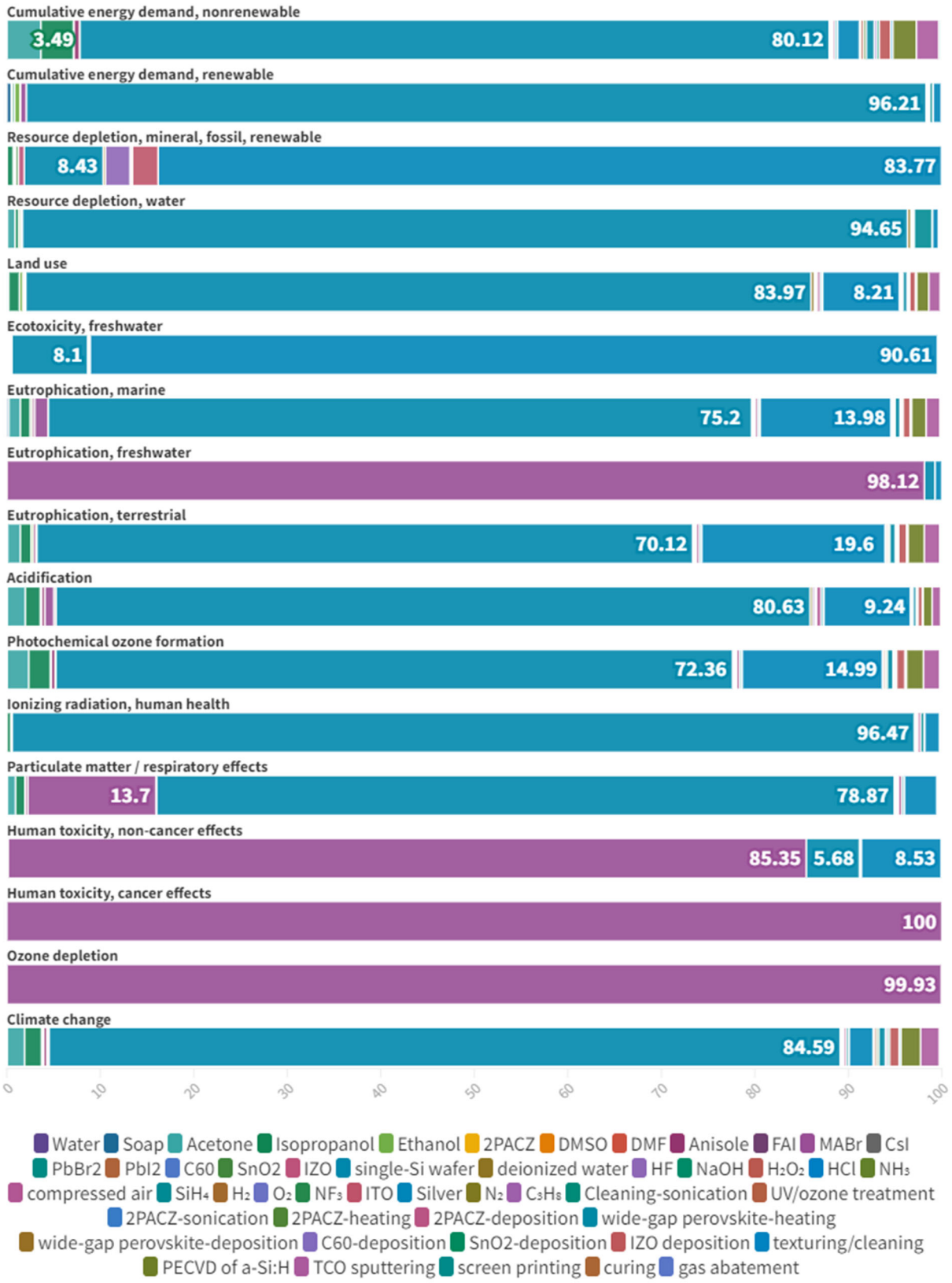
Cumulative energy demand, nonrenewable
3.49
80.12
Cumulative energy demand, renewable
96.21
Resource depletion, mineral, fossil, renewable
8.43
83.77
Resource depletion, water
94.65
Land use
83.97
8.21
Ecotoxicity, freshwater
8.1
90.61
Eutrophication, marine
75.2
13.98
Eutrophication, freshwater
98.12
Eutrophication, terrestrial
70.12
19.6
Acidification
80.63
9.24
Photochemical ozone formation
72.36
14.99
Ionizing radiation, human health
96.47
Particulate matter / respiratory effects
13.7
78.87
Human toxicity, non-cancer effects
85.35
5.68
8.53
Human toxicity, cancer effects
100
Ozone depletion
99.93
Climate change
84.59
0
10
20
30
40
50
60
70
80
90
100
Water
Soap
Acetone
Isopropanol
Ethanol
2PACZ
DMSO
DMF
Anisole
FAI
MABr
CsI
PbBr2
PbI2
C60
SnO2
IZO
single-Si wafer
deionized water
HF
NaOH
H2O2
HCl
NH3
compressed air
SiH4
H2
O2
NF3
ITO
Silver
N2
C3H8
Cleaning-sonication
UV/ozone treatment
2PACZ-sonication
2PACZ-heating
2PACZ-deposition
wide-gap perovskite-heating
wide-gap perovskite-deposition
C60-deposition
SnO2-deposition
IZO deposition
texturing/cleaning
PECVD of a-Si:H
TCO sputtering
screen printing
curing
gas abatement

64

Figure S4. Contribution analysis results for the commercial-scale perovskite-silicon tandem with a "cradle-to-grave" system boundary.

As shown in our previous study,[7] organic solvents would induce substantial environmental impacts if they are not recycled at the EOL or merely incinerated as hazardous waste. To this end, for commercial-scale processes, organic solvents, such as acetone and isopropanol, are considered to be effectively recovered and re-used with an efficiency of approximately 90%, according to the existing literature.[8, 9] Figure S3 and Figure S4 show the environmental profiles of the commercial-scale perovskite-perovskite and perovskite-silicon tandems for the explored midpoint impact categories according to the PEF method, respectively. We note that the overall environmental profile of the commercial-scale perovskite-perovskite tandem looks more dynamic, i.e., the percentage share of each material and processing step is more evenly distributed. The contributions from the identified hotspot material and processing steps are drastically reduced compared to the environmental profiles of the laboratory-scale tandems.

Resistivity test

The resistivity of the ITO substrates was measured using a four-point probe setup consisting of a 2450 Keithley SourceMeter and a four-point collinear probe.

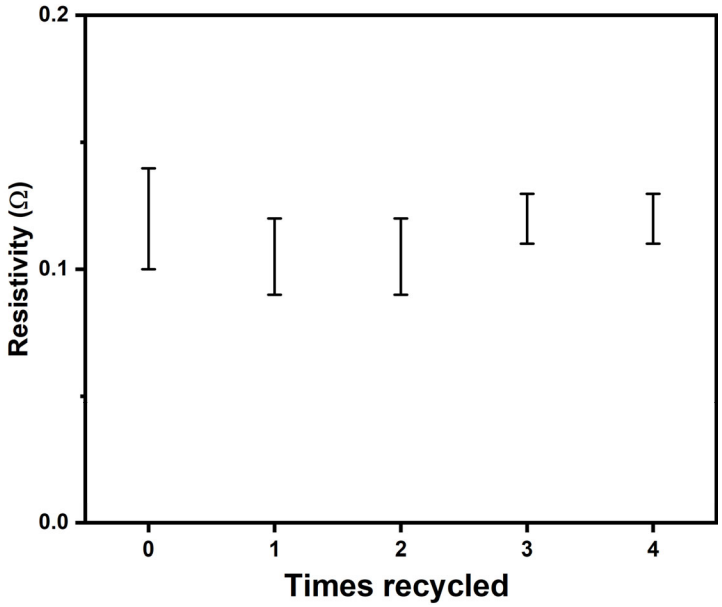

Figure S5. Resistivity test of the pristine and recycled ITO substrates.

Short current density (Jsc), open circuit voltage (Voc), and fill factor (FF) of perovskite-perovskite tandem

Figure S6 shows the short current density, open circuit voltage, and fill factor of perovskite-perovskite

tandem, as a function of times recycled.

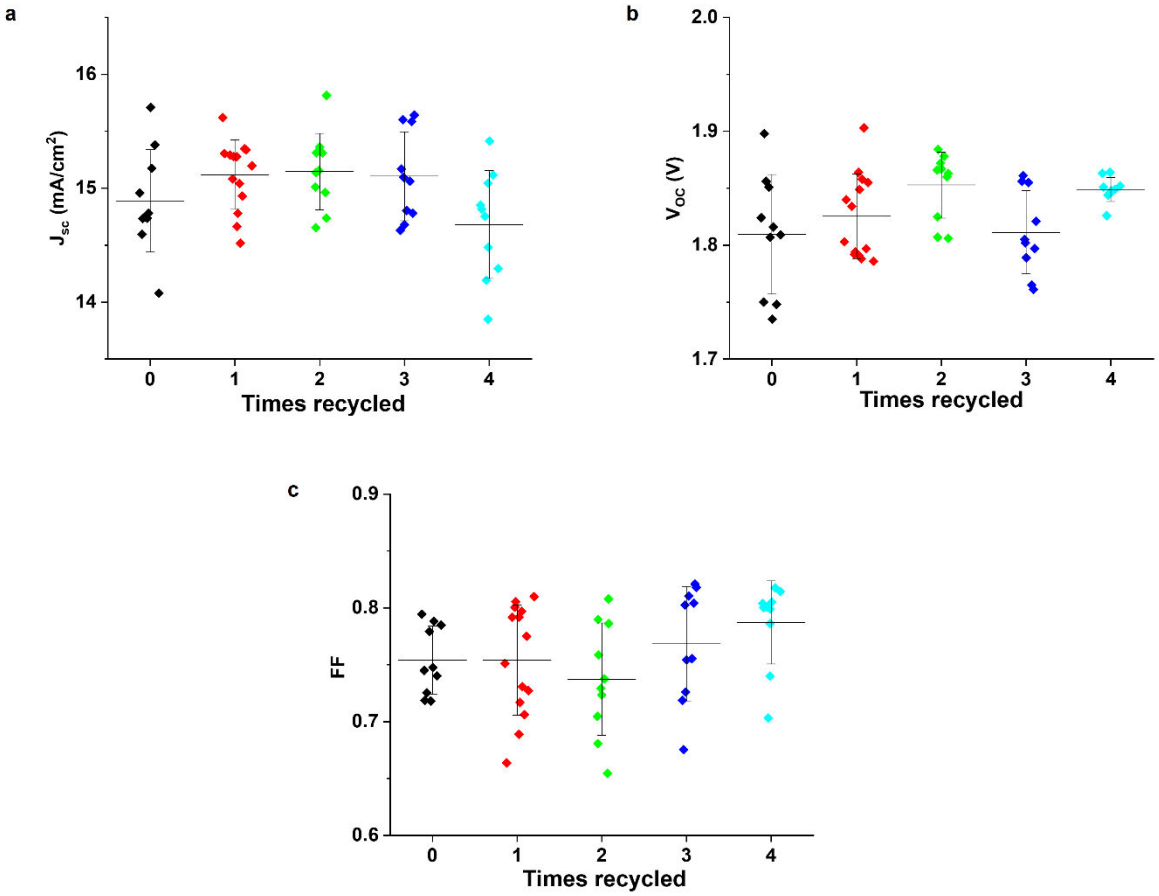

Figure S6. **a**, Short current density (J_{sc}) as a function of times recycled. **b**, Open circuit voltage (V_{oc}) as a function of times recycled. **c**, Fill factor (FF) as a function of times recycled.

Transmittance

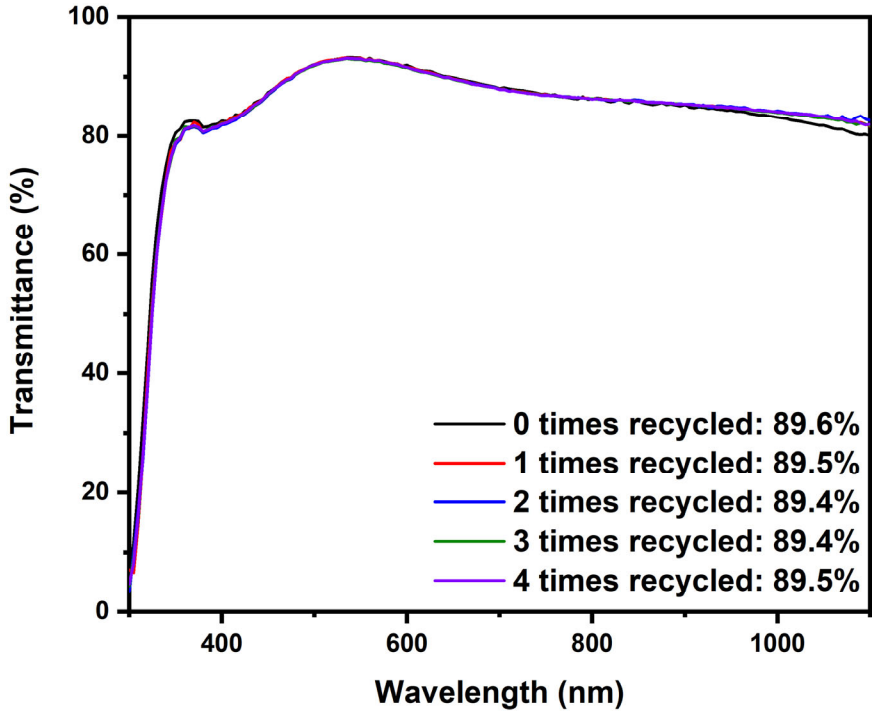

Figure S7. Optical transmittance of substrates before and after recycling. The percentages shown refer to the transmittance of AM1.5G illumination. Loss of transmittance mainly occurs in the 300-400nm range, this is attributed to SnO_x deposition on the front of the substrate during atomic layer deposition. This can likely be prevented in an industrial setting, but even here the overall reduction in transmittance is negligible.

Transmittance was measured using a Bentham PVE300 system in transformer mode. A dual xenon short-arc lamp and a quartz halogen lamp were utilized as the light source, with a swing-away mirror set to 750 nm. A 10 × 10 mm Si reference diode was used as the detector. Transmittance was calculated by dividing the diode response in the presence of a substrate by the diode response without substrate.

Scanning electron microscopy

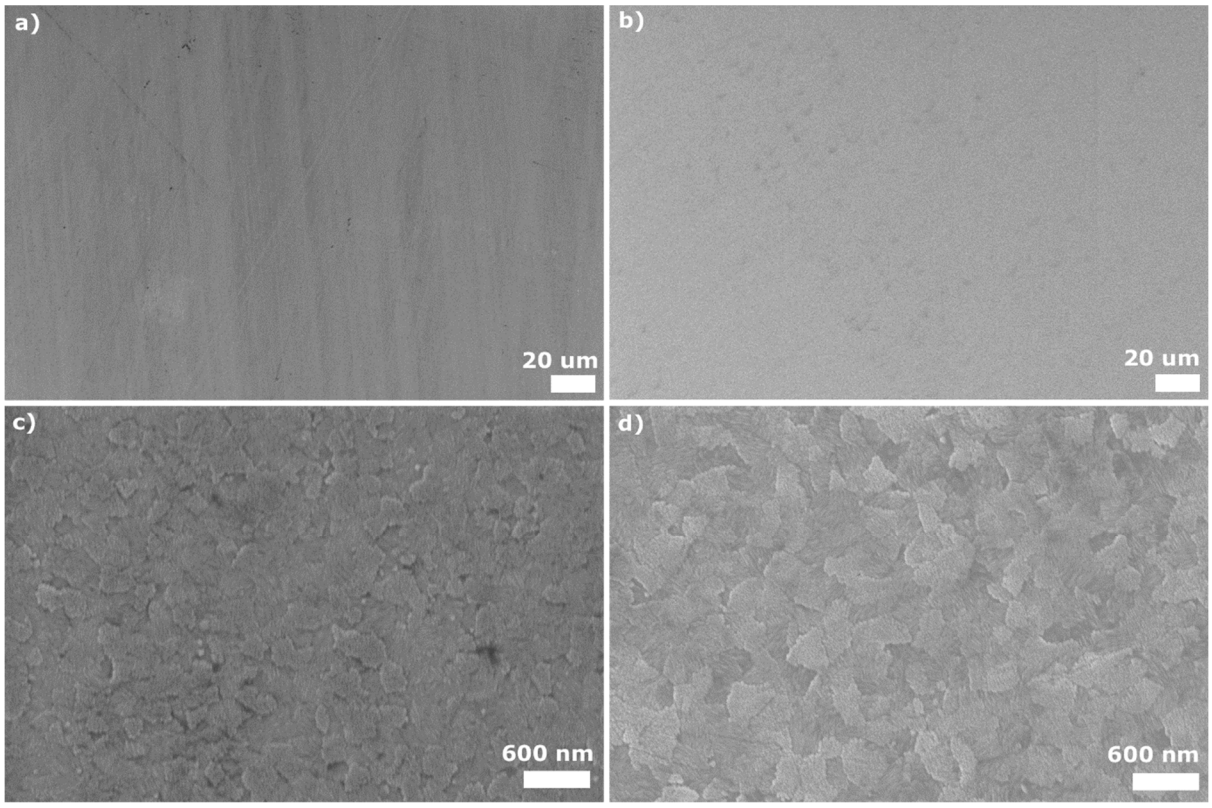

Figure S8. Scanning electron microscope images at 1000X (a,b) and 50000X (c,d) magnification of new (a,c) and recycled substrates (b,d). There are no traces of leftover perovskite on the recycled substrates, showing that the recycling strategy effectively removes all materials from the substrate.

Scanning electron microscopy was performed using a Zeiss LEO 1550 FE-SEM with a field emission source operating at 2 kV acceleration voltage in the InLens mode.

Normalized photoluminescence (PL) intensity and PL quantum efficiency (PLQE)

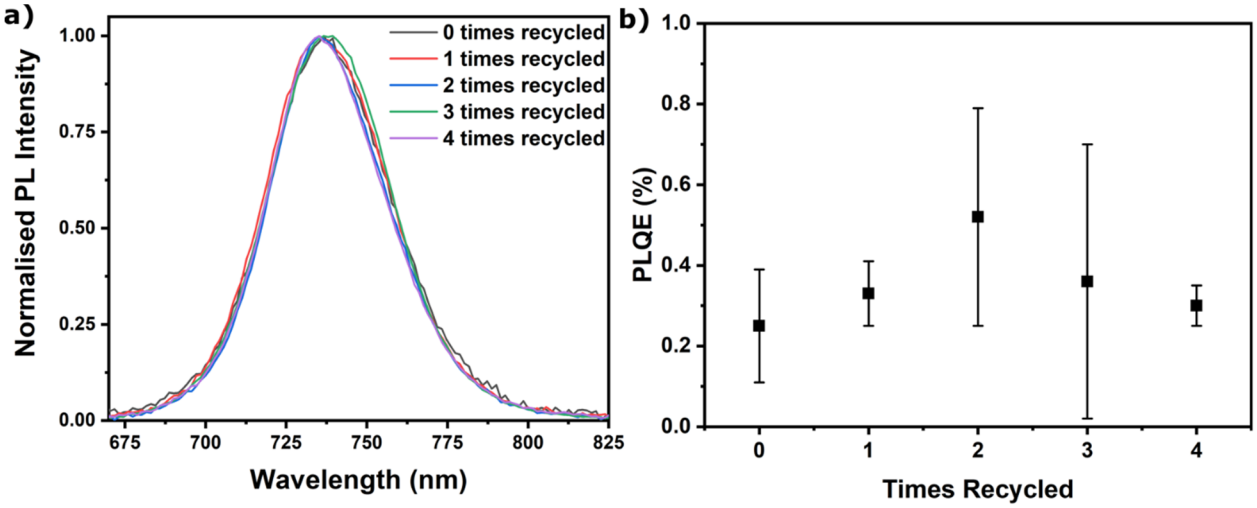

Figure S9. Normalized photoluminescence (PL) intensity (Figure a) and corresponding PL quantum efficiency (Figure b, values are averages for five individual measurements for each recycling frequency) of $Cs_{0.25}FA_{0.75}PbI_{2.1}Br_{0.9}$ perovskite deposited on fresh and recycled substrates. There is no obvious change in peak position and width, or in the PLQE values, indicating that the perovskite quality is not significantly affected by using recycled substrates.

PL and PLQE measurements were recorded using an integrating sphere, following the three-measurement approach of de Mello et al.[10] In both PL and PLQE measurements, a continuous wave temperature-controlled Thorlabs 520 nm laser was used to photoexcite samples. Excitation intensity was varied with an optical filter wheel. The emission was recorded using an Andor IDus DU420A silicon detector.

Solar cell stability test

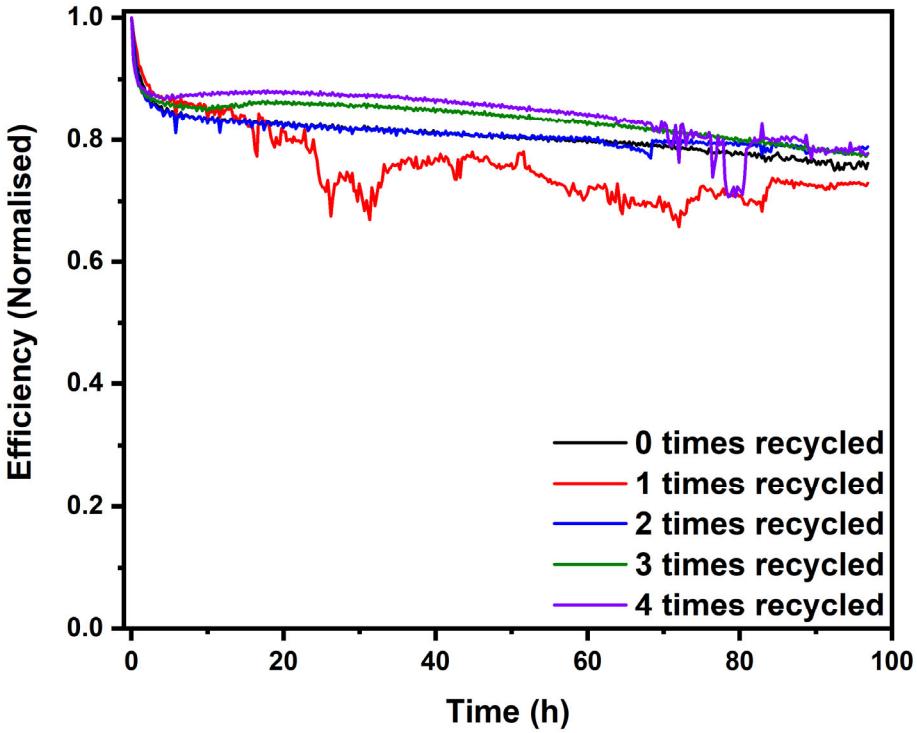

Figure S10. Normalized efficiency of perovskite-perovskite tandem solar cells deposited on fresh and recycled substrates.

A 100-hour maximum power point tracking stability test of fresh and recycled substrates shows that there is no significant change in degradation rate when recycled substrates are used. Although we do not observe any adverse effects of the recycling process on stability on the timescales we have studied, multi-year testing would be required to ensure that the recycling process does not affect stability on the timescales of operation in real-world applications. Each curve is the average of five devices. Devices were encapsulated using glass and UV-curable epoxy glue immediately after fabrication. Stability measurements were carried out under an inert atmosphere and AM1.5G illumination generated by a G2V Base-UV Sunbrick. Maximum power point traces were collected using a 32-channel Arkeo setup (Cicci Research). Further optimization of the layers will improve their absolute stability, but the focus of this study is to demonstrate that the stability remains comparable when considering various numbers of recycling steps.

Cumulative energy yield

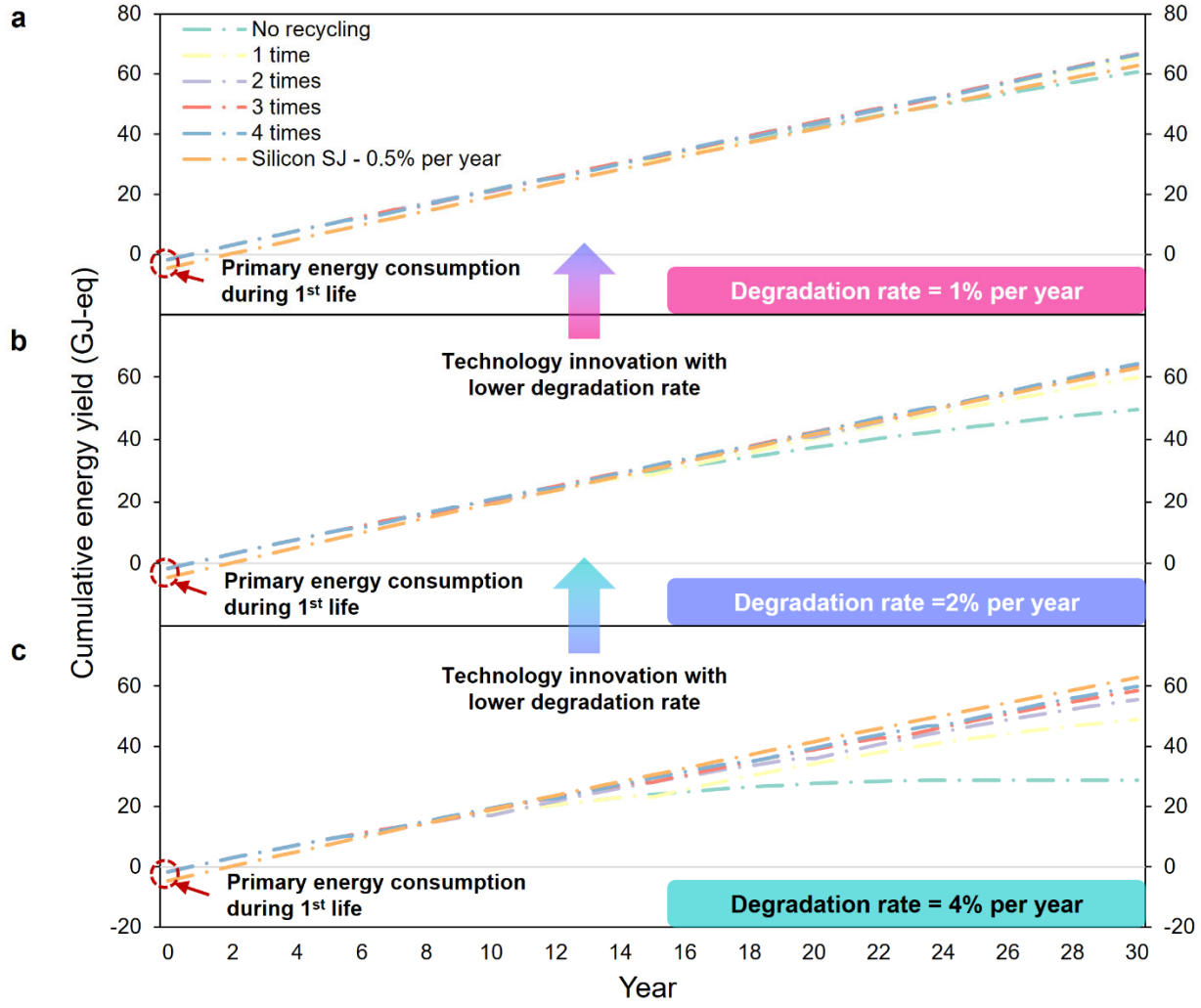

Figure S11. Cumulative energy yield for perovskite-perovskite tandems considering degradation rates of 1%, 2%, and 4% per year. **a**, Cumulative energy yield for perovskite-silicon tandems with different recycling frequencies (from no recycling to four times over the system lifetime) under 1% per year degradation, and compared to the silicon PVs (0.5% per year degradation). **b**, Cumulative energy yield for perovskite-silicon tandems with different recycling frequencies (from no recycling to four times over the system lifetime) under 2% per year degradation and compared to the silicon PVs (0.5% per year degradation). **c**, Cumulative energy yield for perovskite-silicon tandems with different recycling frequencies (from no recycling to four times over the system lifetime) under 4% per year degradation, and compared to the silicon PVs (0.5% per year degradation). The cumulative energy yields initiate as negative values (year zero), which are equal to the initial primary energy consumption.

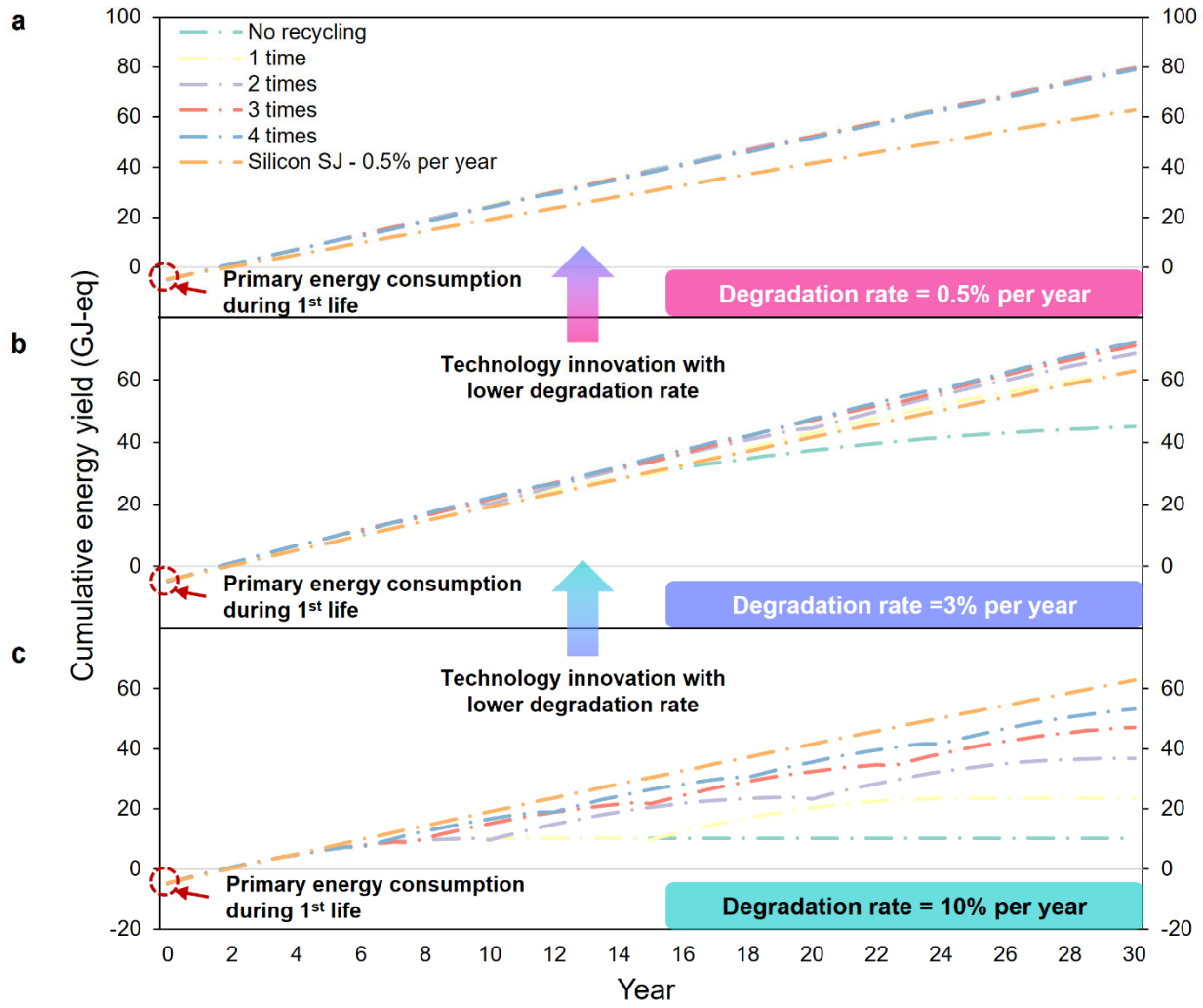

Figure S12. Cumulative energy yield for perovskite-silicon tandems considering degradation rates of 0.5%, 3%, and 10% per year. **a**, Cumulative energy yield for perovskite-silicon tandems with different recycling frequencies (from no recycling to four times over the system lifetime) under 0.5% per year degradation, and compared to the silicon PVs (0.5% per year degradation). **b**, Cumulative energy yield for perovskite-silicon tandems with different recycling frequencies (from no recycling to four times over the system lifetime) under 3% per year degradation and compared to the silicon PVs (0.5% per year degradation). **c**, Cumulative energy yield for perovskite-silicon tandems with different recycling frequencies (from no recycling to four times over the system lifetime) under 10% per year degradation, and compared to the silicon PVs (0.5% per year degradation). The cumulative energy yields initiate as negative values (year zero), which are equal to the initial primary energy consumption.

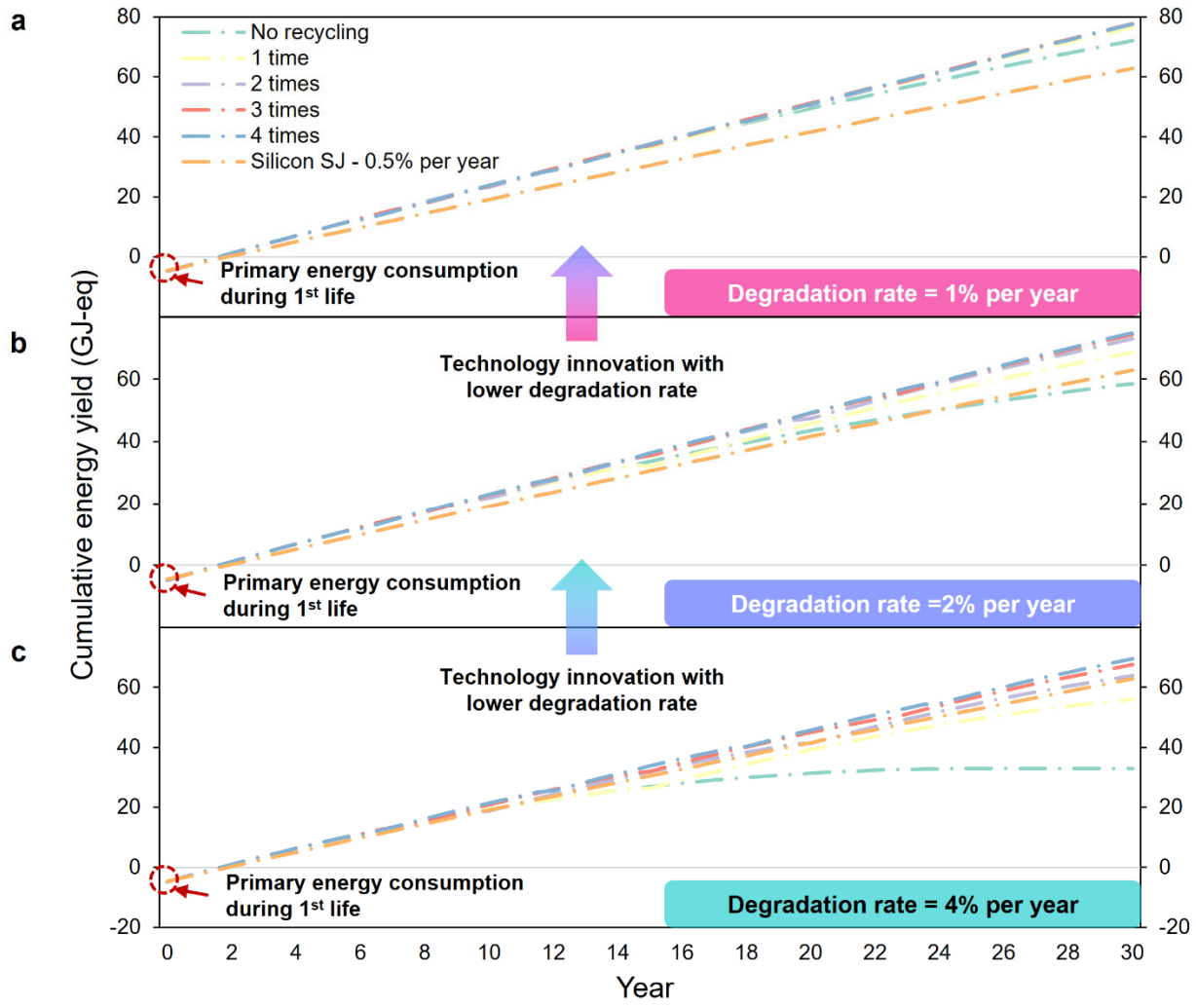

Figure S13. Cumulative energy yield for perovskite-silicon tandems considering degradation rates of 1%, 2%, and 4% per year. **a**, Cumulative energy yield for perovskite-silicon tandems with different recycling frequencies (from no recycling to four times over the system lifetime) under 1% per year degradation, and compared to the silicon PVs (0.5% per year degradation). **b**, Cumulative energy yield for perovskite-silicon tandems with different recycling frequencies (from no recycling to four times over the system lifetime) under 2% per year degradation and compared to the silicon PVs (0.5% per year degradation). **c**, Cumulative energy yield for perovskite-silicon tandems with different recycling frequencies (from no recycling to four times over the system lifetime) under 4% per year degradation, and compared to the silicon PVs (0.5% per year degradation). The cumulative energy yields initiate as negative values (year zero), which are equal to the initial primary energy consumption.

Doctor blading v.s. solvent dissolution method

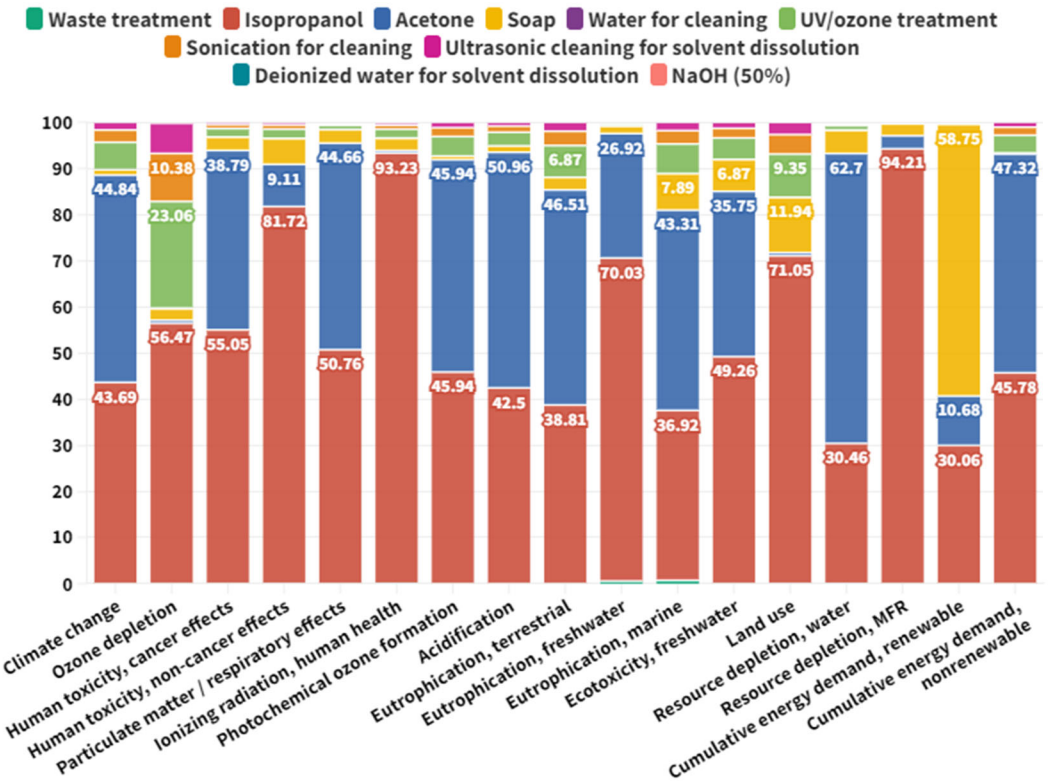

Figure S14. Environmental profile for recycling process based on the solvent dissolution method.

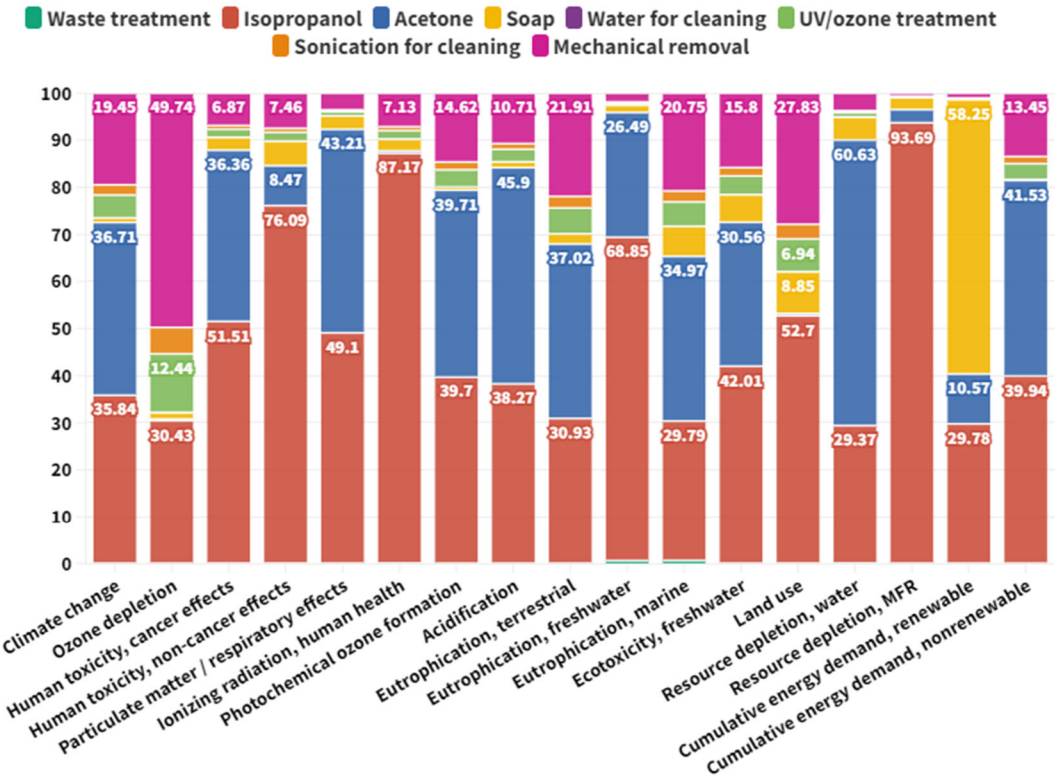

Figure S15. Environmental profile for recycling process based on the blade-scratching method.

Figure S14 and Figure S15 show the environmental profiles for the recycling process based on the solvent dissolution method and the blade-scratching method, respectively. Note that the subsequent cleaning processes are the same for either the solvent dissolution method or the blade-scratching method. Overall, the environmental impact of mechanical removal is more pronounced than solvent dissolution.

Techno-economic analysis for the recovery process with sensitivity analysis

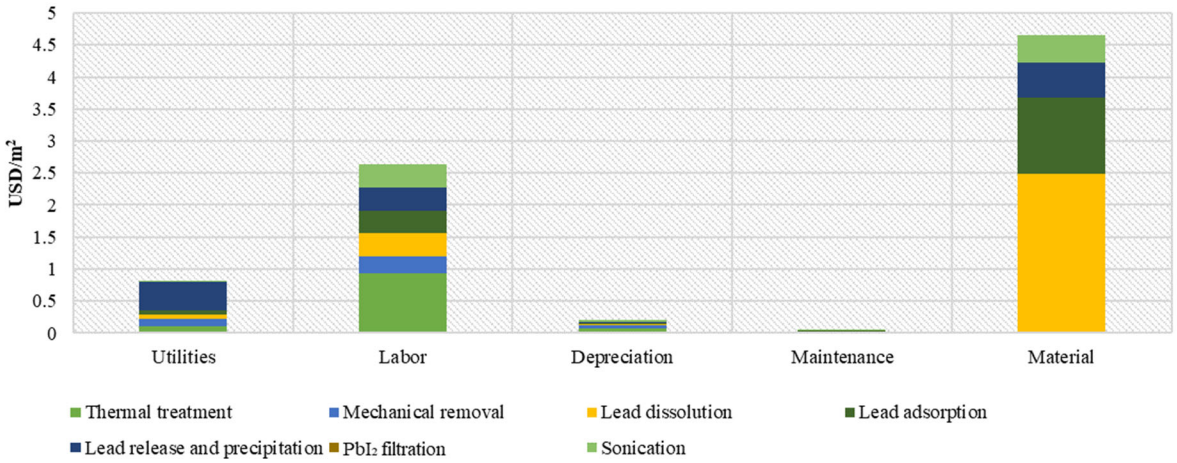

Figure S16. Techno-economic analysis for the recycling process of perovskite-perovskite tandem modules.

Figure S16 shows the techno-economic analysis results for the recycling process of the perovskite-perovskite tandem modules. The results show that the costs in the recovery process of the perovskite-perovskite tandem are dominated by labor (31.6%) and material costs (55.8%), and the total recycling cost is \$ 8.3 / m^2 of the tandem module. A sensitivity analysis is also performed to capture the impact of key parameter variations, including labor cost, electricity price, and other material prices, due to the uncertainty of the recycling process on an industrial scale, as shown in Figure S17. The equipment cost, electricity usage, process throughput, and associated labor cost used for the techno-economic analysis are extracted from existing literature.[11, 12] The maintenance costs for the facilities are assumed to be 20% of the annual equipment depreciation.[13] Material costs are estimated based on recycling process of lead and transparent conductors from perovskite solar modules by Chen et al.[14]

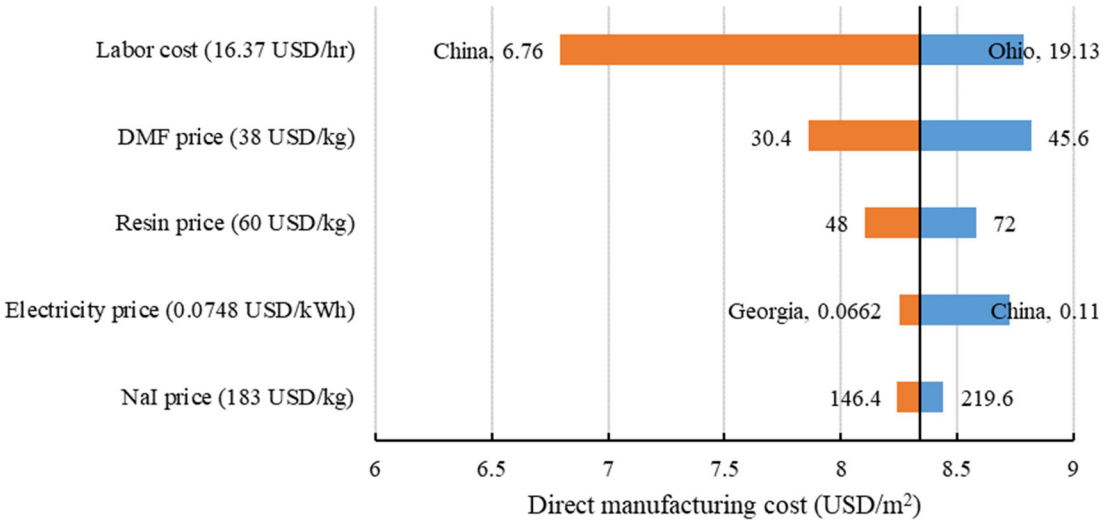

Figure S17. Sensitivity analysis for the recycling cost of perovskite-perovskite tandem modules.

Impact of module shipping

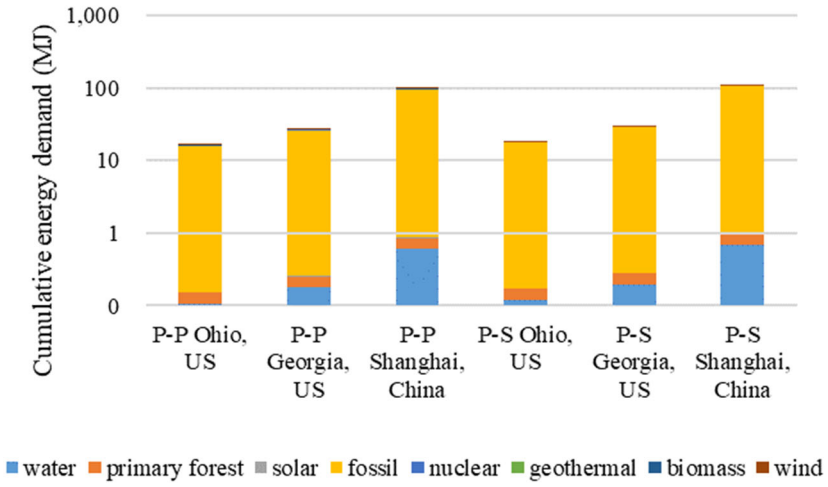

Figure S18. Cumulative energy demand for international and domestic module shipping for the perovskite-perovskite (P-P) and perovskite-silicon (P-S) tandems.

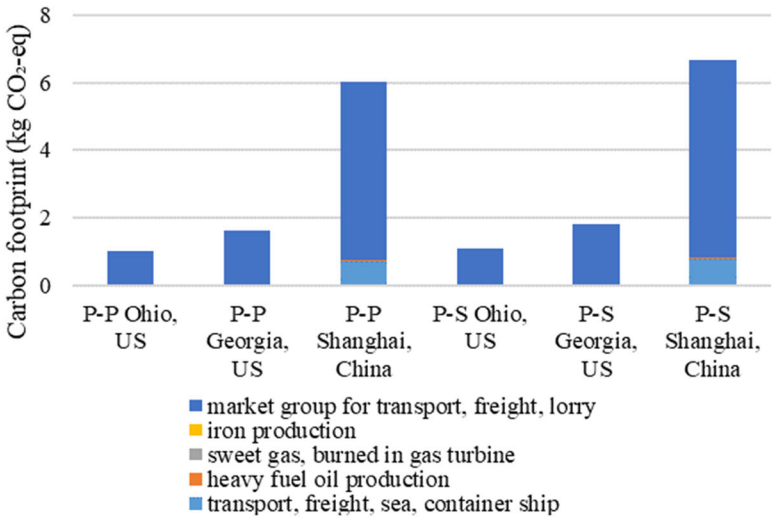

Figure S19. The carbon footprint for international and domestic module shipping for the perovskite-perovskite (P-P) and perovskite-silicon (P-S) tandems.

Figure S18 and Figure S19 show the cumulative energy demand and carbon footprint associated with international and domestic module shipping for the perovskite-perovskite and perovskite-silicon tandems. Specifically, we compare the cumulative energy demand and carbon footprint for three scenarios by assuming that the modules are produced in Ohio State, Georgia State, and Shanghai, China, respectively, and then transported to and installed in New York State, US. The energy cost and GHG emissions are quantified in terms of primary energy forms and involved activities, respectively. The shipping impacts for modules produced and installed in other regions or countries could be estimated in the same way.

Sensitivity analysis of EROI on insolation condition

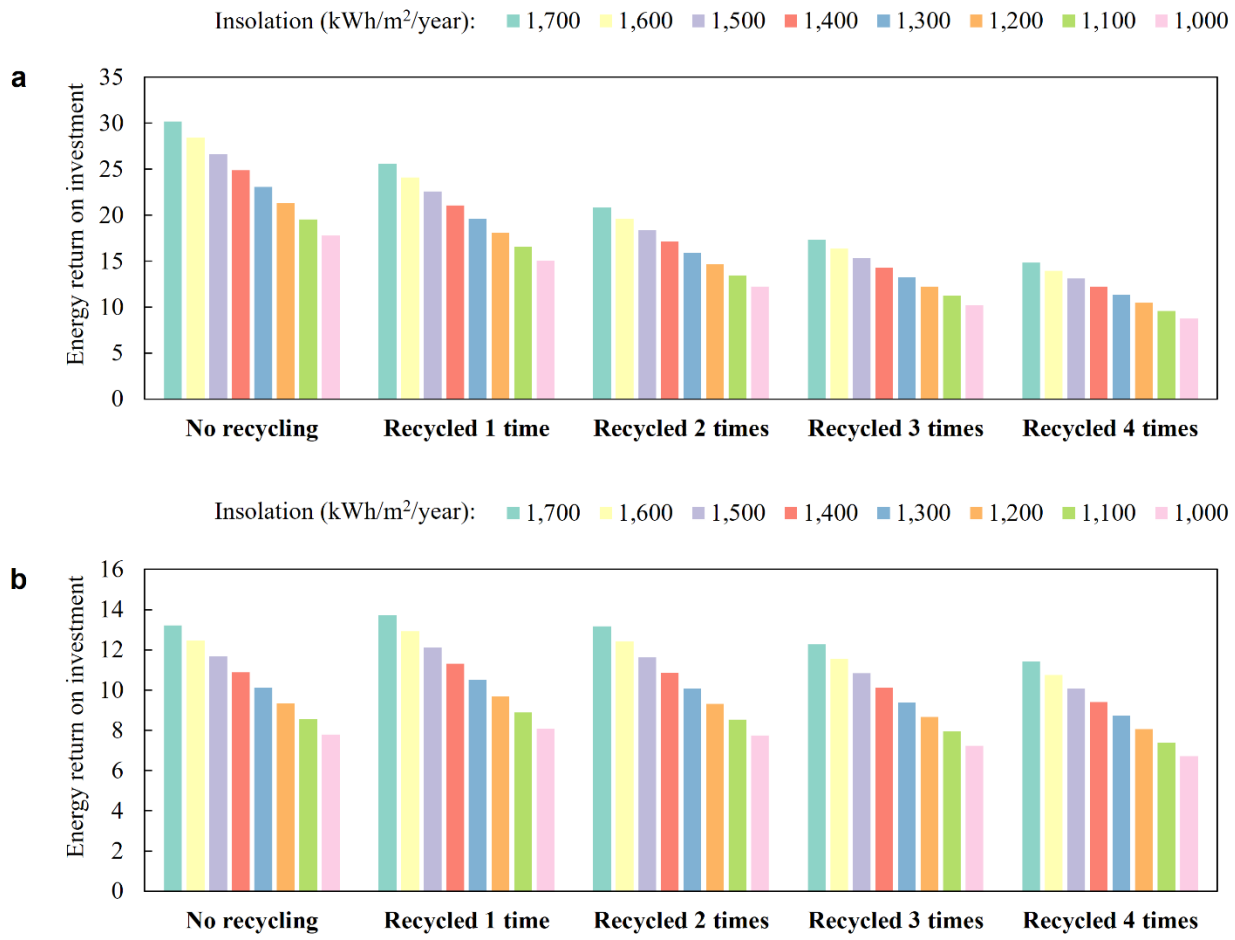

Figure S20. Impact of insolation condition on energy return on investment for perovskite tandems under 2% per year degradation. **a**, Sensitivity of energy return on investment for perovskite-perovskite tandem with a spectrum of insolation conditions, ranging from 1,000 to 1,700 kWh/m^2 per year. **b**, Sensitivity of energy return on investment for perovskite-silicon tandem with a spectrum of insolation conditions, ranging from 1,000 to 1,700 kWh/m^2 per year. The default insolation condition is 1,700 kWh/m^2 per year, and we explore how energy return on investment results would change if worse insolation conditions were assumed.

In this study, nominal insolation of 1,700 kWh/m^2 per year is assumed in the calculation of energy yield potential, energy return on investment (EROI), and greenhouse gas (GHG) emission factor, compliant with the literature.[15] However, this insolation condition is quite favorable for PV and the results would change with different insolation. Figure S20 shows how the EROIs of the explored perovskite tandem stacks with different module replacement strategies vary with different insolation. We note that the EROI of the perovskite-perovskite tandem becomes less sensitive to the change of insolation as the recycling frequency increases, while that of the perovskite-silicon tandem is almost unchanged.

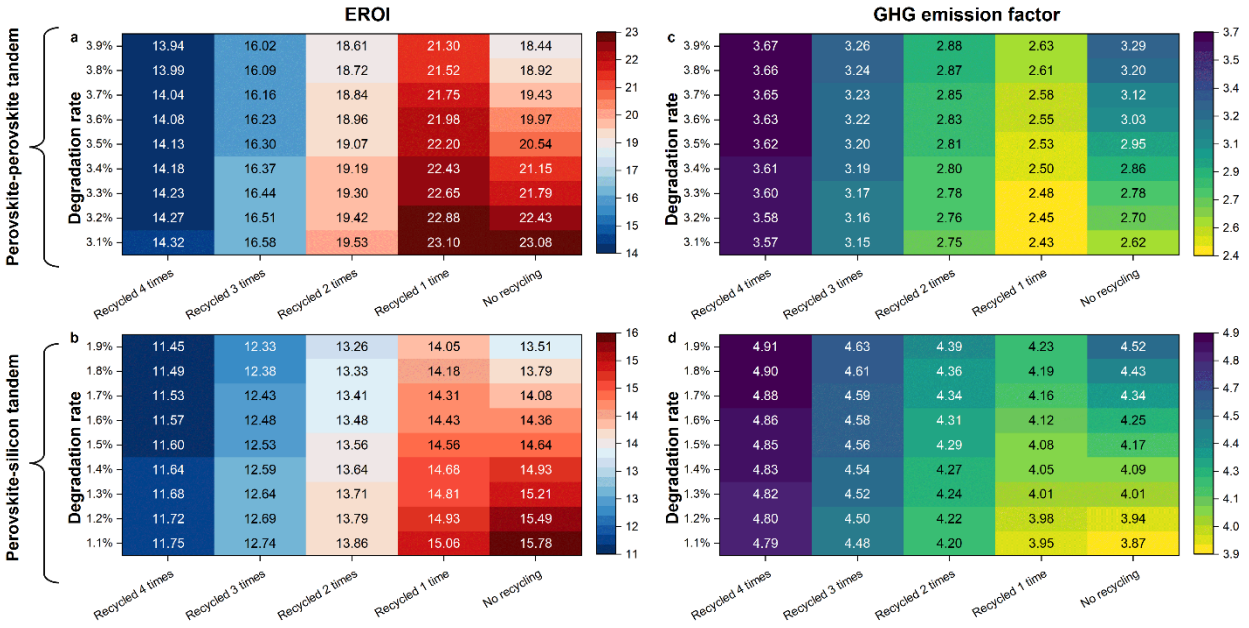

Figure S21. **GHG emission factor (g CO_2-eq/MJ) and EROI for the perovskite-perovskite and perovskite-silicon tandems with periodic module replacement under different module degradation scenarios and recycling frequencies.** The GHG emission factor and EROIs for the two investigated perovskite tandems are estimated under an insolation level of 1,700 kWh m^{-2} per year over a total system lifetime of 30 years. Five scenarios with varying recycling frequencies are simulated, considering the perovskite tandem modules are recycled zero to four times over a total system lifetime of 30 years. For the perovskite-perovskite tandem, the region of interest is from 3.1% to 3.9% per year degradation; for the perovskite-silicon tandem, the region of interest is from 1.1% to 1.9% per year degradation. **a**, Heatmap for EROI of the perovskite-perovskite tandems. **b**, Heatmap for EROI of the perovskite-silicon tandems. **c**, Heatmap for GHG emission factor of the perovskite-perovskite tandems. **d**, Heatmap for GHG emission factor of the perovskite-silicon tandems. The GHG emission factor and EROI of the silicon single junction at 0.5% per year degradation are estimated to be 4.73 g CO_2-eq/MJ and 14.8, respectively.

Impact of PCE threshold on perovskite-perovskite tandem module replacement

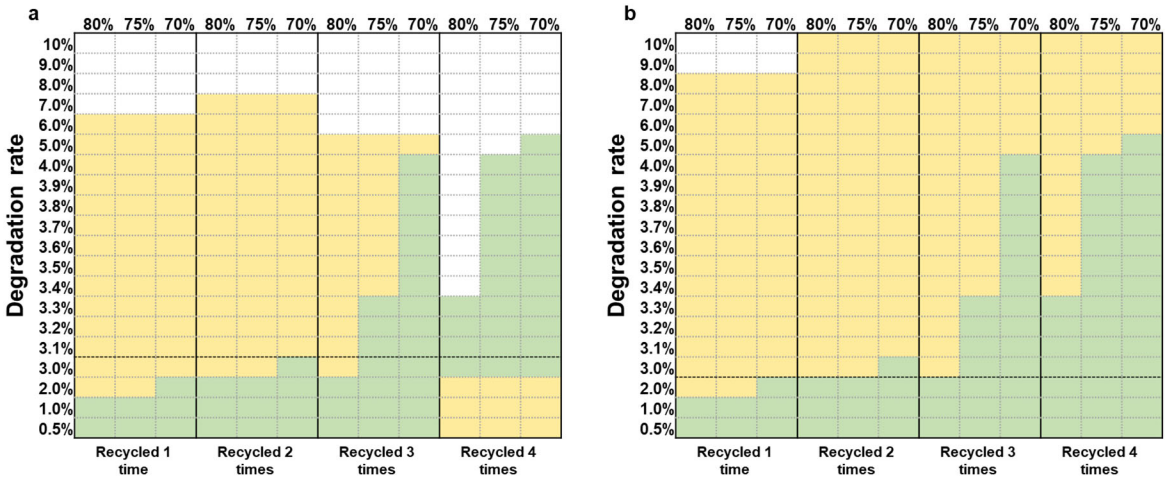

Figure S22. **Impact of PCE threshold on perovskite-perovskite tandem module replacement.** Three scenarios are considered when the threshold is assumed to be 80%, 75%, and 70%. The box in yellow indicates that the corresponding scenario outperforms the reference case of silicon PV in terms of the investigated sustainability metric, namely EROI or GHG emission factor. The box in green represents the replacement scenario is viable given the degradation rate, recycling frequency, and PCE threshold for replacement (the module PCE would not drop below the threshold before being replaced). The dotted line stands for the degradation rate where intermediate recycling is no longer needed. **a**, Feasibility analysis for perovskite-perovskite tandem module replacement in terms of EROI. **b**, Feasibility analysis for perovskite-perovskite tandem module replacement in terms of GHG emission factor.

Figure S22 demonstrates that the module replacement strategy becomes viable in the EROI terms when recycled three times. Specifically, tandem modules with an annual degradation rate of 3.1% to 4.0% can still outperform silicon PV if a 70% replacement threshold is applied, whereas the feasible region narrows to between 3.1% and 3.3% when using a 75% threshold. In terms of the GHG emission factors, a wider region is observed for the perovskite-perovskite tandem to outcompete silicon PV, particularly when recycled more than three times over the 30-year period.

Material and energy inventory

Table S1. Material inventory of 1 m^2 of the perovskite-silicon tandem solar cell.

Process		Unit	Value
Silicon bottom cell fabrication			
Wafer production	Single-Si wafer	m^2	1.00E+00
Texturing/cleaning	Deionized water	kg	3.34E+01
	Hydrogen fluoride	kg	9.50E-02
	Sodium hydroxide	kg	1.56E-01

	Hydrogen peroxide	kg	5.60E-02
	Hydrochloride acid	kg	6.10E-02
	Ammonia	kg	1.10E-02
	Compressed air	m^3	2.50E-01
PECVD of a-Si:H	Deionized water	kg	3.94E+02
	Silane	kg	1.62E-03
	Hydrogen	kg	2.42E-03
	Oxygen	kg	2.60E-04
	NF_3 (for cleaning)	kg	2.20E-03
TCO sputtering	Deionized water	kg	5.12E+02
	ITO	kg	2.74E-03
Screen printing	Compressed air	m^3	1.10E+00
	Silver paste	kg	2.96E-02
Gas abatement	Deionized water	kg	1.20E+01
	Oxygen	kg	5.10E-03
	Nitrogen	kg	4.30E-03
	Propane	kg	3.30E-03
	Compressed air	m^3	1.40E-02
PSC fabrication			
	Water	kg	2.33E+00
	Soap	kg	4.70E-02
	Acetone	kg	1.84E+00
	Isopropanol	kg	1.83E+00
	Ethanol	kg	1.22E-01
	2PACZ	kg	1.33E-06
	DMSO	kg	3.41E-02
	DMF	kg	1.17E-01
	Anisole	kg	3.09E-01
	FAI	kg	6.05E-04
	MABr	kg	1.21E-04
	CsI	kg	6.05E-05
	$PbBr_2$	kg	7.34E-04
	PbI_2	kg	1.15E-03
	C_{60}	kg	4.40E-05
	TDMASn	kg	8.69E-04
	IZO	kg	6.99E-04
Encapsulation			

	Solar glass	kg	8.53E+00
	PET	kg	7.28E-02
	Adhesive	kg	5.06E-02
Landfill		kg	9.60E+00

Table S2. Energy inventory of 1 m^2 of the perovskite-silicon tandem solar cell.

Process	Electricity (kWh)
SHJ cell fabrication	
Texturing/cleaning	6.47E-01
PECVD of a-Si:H	6.59E+00
TCO sputter	6.30E+00
Screen printing	5.24E-01
Curing	3.10E-01
Gas abatement	4.50E-02
PSC fabrication	
Cleaning-sonication	3.49E-01
UV/ozone treatment	7.75E-01
2PACZ deposition-sonication	7.75E-03
2PACZ deposition-heating	7.50E-01
2PACZ deposition-screen printing	1.07E-02
wide-gap perovskite-heating	2.25E+00
wide-gap perovskite-screen printing	1.07E-02
C_{60}-deposition	6.82E-01
SnO_2-deposition	7.02E-01
IZO-deposition	3.21E+00
Encapsulation	6.68E-03
Mechanical removal	3.10E+00
Total	**26.3**

Table S1 and Table S2 summarize the material and energy inventory for fabricating 1 m^2 of the perovskite-silicon tandem solar cell, respectively. Specifically, the material and energy inventory for depositing the silicon bottom cell (silicon heterojunction solar cell) in the tandem stack is retrieved from the literature.[16] The detailed mass and energy balances for perovskite sub-cell deposition are derived based on the data generated at the laboratory scale. Our estimates of energy inputs during the recycling process (based on a roll-to-roll blade coater with 10-second operations for active layer removal)[17] serve as the upper bound for the real-world application as we are not recuperating much of the end-of-life tandem modules (merely re-using ITO-coated glass), and the energy consumption is scaled based on the “best available”

288 data obtained at laboratory scale. All devices used for assembling the perovskite-silicon solar cells were
289 driven by electricity, and the amount of electricity consumption in each procedure was evaluated based on
290 power and corresponding operational time. Electricity consumption for manufacturing and recycling 1 m^2 of
291 the perovskite-silicon tandem amounted to 26.3 kWh.
292

293 Table S3. Material inventory of 1 m^2 of the perovskite-perovskite tandem solar cell.

Process	Unit	Value
ITO glass	m^2	1.00E+00
Water	kg	2.33E+00
Soap	kg	4.70E-02
Acetone	kg	1.84E+00
Isopropanol	kg	1.83E+00
Ethanol	kg	1.22E-01
2PACZ	kg	1.33E-06
DMSO	kg	4.26E-02
DMF	kg	1.10E-01
Methyl acetate	kg	2.90E-01
FAI	kg	5.57E-04
CsI	kg	2.82E-04
$PbBr_2$	kg	7.14E-04
PbI_2	kg	1.11E-03
C_{60}	kg	4.40E-05
SnO_2	kg	8.69E-04
Gold	kg	2.57E-05
Methanol	kg	1.84E-01
Water	kg	7.75E-02
PEDOT:PSS	kg	4.24E-05
DMSO	kg	4.26E-02
DMF	kg	1.10E-01
Anisole	kg	3.09E-01
FAI	kg	1.29E-03
CsI	kg	3.46E-04
PbI_2	kg	2.04E-03
SnI_2	kg	1.65E-03
C_{60}	kg	4.40E-05
BCP	kg	1.12E-05
Cu	kg	1.40E-03
Encapsulation		
Solar glass	kg	8.53E+00
PET	kg	7.28E-02
Adhesive	kg	5.06E-02
Landfill	kg	8.66E+00

Table S4. Energy inventory of 1 m^2 of the perovskite-perovskite tandem solar cell.

Process	Electricity (kWh)
Fabrication	
Cleaning-sonication	3.49E-01
UV/ozone treatment	7.75E-01
2PACZ deposition-sonication	7.75E-03
2PACZ deposition-heating	7.50E-01
2PACZ deposition-screen printing	1.07E-02
Wide-gap perovskite-heating	2.25E+00
Wide-gap perovskite-screen printing	1.07E-02
C_{60}-deposition	1.36E+00
SnO_2-deposition	7.02E-01
Gold-deposition	3.55E-01
PEDOT:PSS-heating	1.35E+00
PEDOT:PSS-screen printing	1.07E-02
Low-gap perovskite-heating	7.50E-01
Low-gap perovskite-screen printing	1.07E-02
BCP-deposition	2.47E-01
Copper-deposition	5.71E+00
Encapsulation	6.68E-03
Mechanical removal	3.10E+00
Total	**17.8**

Table S3 and Table S4 summarize the material and energy inventory for fabricating 1 m^2 of the perovskite-perovskite tandem solar cell, respectively. The detailed mass and energy balances for wide-gap perovskite sub-cell and low-gap perovskite sub-cell deposition are derived based on the data generated at the laboratory scale. Electricity consumption for manufacturing and recycling 1 m^2 of the perovskite-perovskite tandem amounted to 17.8 kWh.

Supplemental references

1. S. Manfredi, K. Allacker, N. Pelletier, K. Chomkhamsri and D. M. de Souza, 2012.
2. A. Al-Ashouri, E. Köhnen, B. Li, A. Magomedov, H. Hempel, P. Caprioglio, J. A. Márquez, A. B. M. Vilches, E. Kasparavicius, J. A. Smith, N. Phung, D. Menzel, M. Grischek, L. Kegelmann, D. Skroblin, C. Gollwitzer, T. Malinauskas, M. Jošt, G. Matič, B. Rech, R. Schlatmann, M. Topič, L. Korte, A. Abate, B. Stannowski, D. Neher, M. Stolterfoht, T. Unold, V. Getautis and S. Albrecht, *Science*, 2020, **370**, 1300-1309.
3. R. Lin, J. Xu, M. Wei, Y. Wang, Z. Qin, Z. Liu, J. Wu, K. Xiao, B. Chen and S. M. Park, *Nature*, 2022, **603**, 73-78.
4. E. Leccisi and V. Fthenakis, *Progress in Photovoltaics: Research and Applications*, 2021, **29**, 1078-1092.
5. N. Espinosa, R. Garcia-Valverde, A. Urbina and F. C. Krebs, *Solar Energy Materials and Solar Cells*, 2011, **95**, 1293-1302.
6. D. Munoz-Rojas and J. MacManus-Driscoll, *Materials Horizons*, 2014, **1**, 314-320.
7. X. Tian, S. D. Stranks and F. You, *Nature Sustainability*, 2021, **4**, 821–829.
8. N. A. Weires, A. Johnston, D. L. Warner, M. M. McCormick, K. Hammond and O. M. McDougal, *Journal of Chemical Education*, 2011, **88**, 1724-1726.
9. S. H. Lin and C. S. Wang, *Journal of Hazardous Materials*, 2004, **106**, 161-168.
10. J. C. de Mello, H. F. Wittmann and R. H. Friend, *Advanced Materials*, 1997, **9**, 230-232.
11. N. L. Chang, A. W. Yi Ho-Baillie, P. A. Basore, T. L. Young, R. Evans and R. J. Egan, *Progress in Photovoltaics: Research and Applications*, 2017, **25**, 390-405.
12. J. Zhang, N. Chang, C. Fagerholm, M. Qiu, L. Shuai, R. Egan and C. Yuan, *Renewable and Sustainable Energy Reviews*, 2022, **158**, 112146.
13. Z. Song, C. L. McElvany, A. B. Phillips, I. Celik, P. W. Krantz, S. C. Watthage, G. K. Liyanage, D. Apul and M. J. Heben, *Energy & Environmental Science*, 2017, **10**, 1297-1305.
14. B. Chen, C. Fei, S. Chen, H. Gu, X. Xiao and J. Huang, *Nature Communications*, 2021, **12**, 5859.
15. V. Fthenakis and E. Leccisi, *Progress in Photovoltaics: Research and Applications*, 2021, **29**, 1068-1077.
16. A. Louwen, W. G. J. H. M. van Sark, R. E. I. Schropp, W. C. Turkenburg and A. P. C. Faaij, *Progress in Photovoltaics: Research and Applications*, 2015, **23**, 1406-1428.
17. *MTI Corporation*, https://www.mtixtl.com/MSK-AFA-MC200.aspx, Apr 7th, 2022.